Applied Surface Science 257 (2011) 9177–9182

Contents lists available at ScienceDirect

Applied Surface Science

journal homepage: www.elsevier.com/locate/apsusc

Insight into the thermionic emission regimes under gold film thermal relaxation excited by a femtosecond pulse

Guangqing Du[a], Qing Yang[b], Feng Chen[a,*], Jinhai Si[a], Xun Hou[a]

[a] Key Laboratory for Physical Electronics and Devices of the Ministry of Education and Key Laboratory of Photonics Technology for Informations, Shaanxi Province, School of Electronics and Information Engineering, Xi'an Jiaotong University, No.28, Xianning West Road, Xi'an 710049, PR China
[b] State Key Laboratory for Manufacturing Systems Engineering, Xi'an Jiaotong University, No. 28, Xianning West Road, Xi'an 710049, PR China

ARTICLE INFO

Article history:
Received 1 March 2011
Received in revised form 31 May 2011
Accepted 31 May 2011
Available online 7 June 2011

Keywords:
Femtosecond laser pulse
Thermionic emission regimes
Two temperature relaxation
Thermal diffusion relaxation

ABSTRACT

We theoretically investigated different thermal relaxation participating in the ultrafast thermionic emission processes on gold film surface with a femtosecond pulse excitation. The thermionic emission regimes under the two temperature relaxation and the thermal diffusion relaxation were demonstrated. The simulations showed that the thermionic emission properties can be defined in the regime under two temperature relaxation by reducing the laser fluence, or widening the pulse duration or increasing the laser wavelength. It was also found that there exists a transition between the two distinct thermionic emission regimes under peculiar laser parameters of laser fluence, pulse duration and laser wavelength. The results were explained as significant intervene of laser irradiation parameters into gold film thermal relaxation processes.

1. Introduction

Pulsed laser excitation of solid target and the electron emission has found a number of potential applications in the fields such as X-ray lasers, high quality photocathodes and laser driven ultrafast electron switches [1–3]. Recently, with progress of laser systems, especially those based on the chirped pulse amplification (CPA) technique, the laser pulse duration can be varied from several nanoseconds to about a few femtosecond (10^{-15}S) and the intensity can be up to 10^{21} W/m^2. Subsequently, the femtosecond laser induced photoelectron and thermion for different applications is therefore widely investigated for basic and practical researches [4–8]. It is generally considered that the photoelectron emission occurs during the pulse duration period, which is inherently beneficial for generation of the ultrashort electron pulse source, particularly when the femtosecond laser is applied. However, the thermionic emission assisted by surface electron temperature predominantly takes place in material thermal relaxation periods, leading to significant complexity of the produced pulse electron profiles.

Until now, the thermionic emission from all kinds of materials such as metals, semiconductors and dielectrics under femtosecond laser pulse excitation have been intensely investigated by many groups [9–11]. Most of the researches referring to the theory of the ultrafast thermionic emission are mainly based on the non-equilibrium two temperature relaxation model, mathematically described by the well-known two temperature equations, which considered the electron or carrier and the phonon as two different temperatures. Earlier, Mao [12] applied the two temperature model and Richard theory to predict the thermionic emission from semiconductors. Later on, the thermionic emission characteristics from a gold film under femtosecond laser pulses irradiation with consideration of enhanced two temperature model was theoretically investigated by Balasubramni et al. [13]. In spite of the previous works, the energy transfer beyond the two temperature relaxation regime for the thermionic emission investigation is still a less touched field. Further studies revealed that, after the two temperature relaxation, the electron and phonon sub-systems get the thermal equilibrium state and the thermal diffusion relaxation dominates the thermal transfer [14,15]. If surface temperature of the target at termination of the two temperature relaxation can be still high enough for exciting thermionic emission, the thermionic emission trends to continue during the thermal diffusion relaxation period, which is extremely unfavorable for generation of ultrashort electron pulses. On the contrary, when the laser parameters are suitably applied, the following thermionic emission regime after the two temperature relaxation termination would be extinguished. For most of the applications, the picosecond and even femtosecond pulse electron is desired, therefore, it becomes significant to regulate the thermionic emission regime in order to satisfy specific application for generation of various kinds of ultrashort electron pulses.

* Corresponding author. Tel.: +86 29 82663485; fax: +86 29 82663485.
E-mail address: chenfeng@mail.xjtu.edu.cn (F. Chen).

0169-4332/$ – see front matter © 2011 Elsevier B.V. All rights reserved.
doi:10.1016/j.apsusc.2011.05.128

In this paper, we theoretically investigated different thermal relaxation participating in the thermionic emission processes on gold film under ultrashort laser pulse excitation. As the thermionic emission can actually occur beyond the two temperature relaxation period, we proposed the temporally sequential thermal relaxation model for predicting full properties of the thermionic emission. The characteristics for thermionic emission regimes under different thermal relaxation of two temperature relaxation and thermal diffusion relaxation were examined in detail. The results provide a way for optimizing the thermionic electron profiles via intervening gold film thermal relaxation processes by adjusting the laser parameters.

2. Modeling and method

The proposed model considers the temporally sequential thermal relaxation, the space charge limited thermionic emission and the temperature dependent thermal and optical properties of the gold target. The thermionic emission is taken as the thermal loss boundary condition on the front surface of the gold film for determination of the gold film melting thresholds. The detailed pieces of the model are described in the following sections.

2.1. Temporally sequential thermal relaxation model

The Fourier thermal diffusion equation is coupled into the well-known two temperature models in order to explore the full thermal relaxation properties for the gold target. It had been proved that the two temperature relaxation plays a major role on timescale of several picoseconds [16–20], but the normal thermal diffusion relaxation mechanism will dominate the main heat transfer after the two temperature relaxation termination. The proposed model is described as

$$C_e\frac{\partial T_e}{\partial t} = \nabla(K_e\nabla T_e) - G(T_e - T_p) + Q \tag{1}$$

$$C_p\frac{\partial T_p}{\partial t} = G(T_e - T_p) \tag{2}$$

$$C\frac{\partial T}{\partial t} = \nabla(K\nabla T) - \varepsilon\sigma(T^4 - T_0^4)d^{-1} \tag{3}$$

The coupled Eqs. (1) and (2) describe the laser energy deposition and the following two temperature relaxation. After the two temperature relaxation termination, the Fourier thermal diffusion relaxation is represented by Eq. (3). The variables T_e and T_p denotes the electron and phonon temperatures, respectively. T is the united electron and phonon temperature at electron–phonon equilibrium state. ε is the emissivity taken as 0.03, σ is the Stefan–Boltzmann constant, the gold film thickness d is considered as 1 μm here, and T_0 is the ambient air temperature taken as 300 K in room temperature.

The energy absorption rate Q is written as

$$Q(x) = \sqrt{\frac{4\ln 2}{\pi}}\frac{1-R}{t_p(\delta+\delta_b)}F \times \exp\left(-\frac{x}{\delta+\delta_b} - 4\ln 2\left(\frac{t-2t_p}{t_p}\right)^2\right) \tag{4}$$

here R is the gold film surface reflectivity, which is temperature and wavelength dependent parameter, t_p is the FWHM pulse duration, δ is the temperature and wavelength dependent optical penetration depth, and δ_b is the electron ballistic transfer length for gold film. F is the laser fluence which can be taken as the optional values in our simulations.

The temperature dependent electron heat capacity can be written as the following piecewise function:

$$C_e(T_e) = \begin{cases} B_eT_e & (T_e < T_F/\pi^2) \\ 2B_eT_e/3 + C_e'/3 & (T_F/\pi^2 \le T_e < 3T_F/\pi^2) \\ n_ek_B + C_e'/3 & (3T_F/\pi^2 \le T_e < T_F) \\ 3n_ek_B/2 & (T_e \ge T_F) \end{cases} \tag{5}$$

here

$$C_e' = B_eT_F/\pi^2 + \frac{3n_ek_B/2 - B_eT_F/\pi^2}{T_F - T_F/\pi^2}(T_e - T_F/\pi^2) \tag{6}$$

Here, the phonon thermal heat capacity C_p and the thermal capacity C at electron–phonon equilibrium is actually less sensitive to ambient temperature on the timescale of several nanosecond, therefore taken as the temperature independent parameters in the calculations.

For a wide range of electron temperature ranging from 300 K to Fermi temperature, temperature dependent electron heat conductivity during two temperature relaxation period is expressed as [21]:

$$K_e(T_e, T_p) = \chi\frac{(\theta_e^2 + 0.16)^{5/4}(\theta_e^2 + 0.44)\theta_e}{(\theta_e^2 + 0.092)^{1/2}(\theta_e^2 + \eta\theta_p)} \tag{7}$$

here $\theta_e = T_e/T_F$ and $\theta_p = T_p/T_F$ are the normalized electron and phonon temperature with T_F denoting the Fermi temperature; χ, η are material constants. The heat conductivity in electron–phonon equilibrium state after the two temperature relaxation can be found to be as follows:

$$K(T) = 320.973 - 0.0111\times T - 2.747\times 10^{-5}\times T^2 - 4.048\times 10^{-9}\times T^3 \tag{8}$$

An analytical expression of the electron–phonon coupling strength was proposed by Zhang and Chen [22], which can be represented as follows:

$$G(T_e, T_p) = G_0\left[\frac{A_e}{B_p}(T_e + T_p) + 1\right] \tag{9}$$

where, G_0 is the electron–phonon coupling strength in room temperature, and the coefficients A_e and B_p are constants.

2.2. Thermionic emission model (TEM)

The thermionic emission rate J, neglecting space–charge fields, can be described by the well-known Richardson–Dushman equation

$$J = C(k_BT_e)^2\exp\left[\frac{-E_f + e\phi - \mu}{k_BT_e}\right] \tag{10}$$

where k_B is the Boltzmann constant, E_f is the Fermi energy, and $C = m/2\pi^2\hbar^3$ where m is the mass of the electron and $\hbar$ is the reduced Plank constant, ϕ is the work function of metal target.

As the surface electron temperature of metal is high enough that a large region of the electron cloud is formed over the surface, the space–charge (SC) effect would play an important role. Because of the complexity of the SC effect, it is large challenge to accurately predict SC limited thermionic emission. An approximate estimation of the SC limited thermionic emission yield can be derived as follows [23]:

$$Y_{\mathrm{esc}} = \frac{k_BT_{\mathrm{peak}}}{ae^2/R_1}\log\left[1 + C\tau\pi R_2ae^2k_BT_{\mathrm{peak}}\ \exp\left(-\frac{E_f - \mu + e\phi}{k_BT_{\mathrm{peak}}}\right)\right] \tag{11}$$

here T_{peak} is the peak electron temperature, τ is the pulse duration for a full width at 80% of T_{peak}, R_1 and R_2 refer to the full width

at half maximum (FWHM) radii of the elliptical spot size of the electron cloud.

2.3. Temperature dependent optical properties

In this study, the Drude model for the plasma in the metals is used to determine the optical properties of the excited target. The temperature dependent complex dielectric function can be split into the real and imaginary parts as follows:

$$\varepsilon = 1 - \frac{\omega_p^2}{\omega^2 + \nu_m^2} + i\frac{\nu_m}{\omega}\frac{\omega_p^2}{\omega^2 + \nu_m^2} \tag{12}$$

where $\omega_p^2 = e^2 n_e/\varepsilon_0 m_e$ denotes the plasma frequency. According to Matthiessen's rule within the relaxation time approximation, the total scattering rate of electrons is the sum of the rates of the separate mechanisms: $\nu_m = 1/\tau_{ee} + 1/\tau_{ep}$, where τ_{e-e} and τ_{e-p} are the electron–electron and electron–phonon scattering times, which actually is temperature dependent parameters, described as $1/A_e T_e^2$ and $1/B_p T_p$, respectively. Considering the relationship between complex reflective index, n_c and the complex dielectric function, $n_c = \sqrt{\varepsilon} = \sqrt{\varepsilon_1 + i\varepsilon_2}$, and applying the Fresnel law at the surface, we get the temperature dependent surface reflectivity coefficient:

$$R(T_e, T_p, \omega) = \frac{[Re(n_c) - 1]^2 + [Im(n_c)]^2}{[Re(n_c) + 1]^2 + [Im(n_c)]^2} \tag{13}$$

The temperature dependent optical penetration depth of laser intensity into the metal plasma is calculated by

$$\delta(T_e, T_p, \lambda) = \left[\frac{2\omega Im(n_c)}{c}\right]^{-1} \tag{14}$$

2.4. Initial and boundary conditions

Because of the flexibility of finite element method (FEM) in dealing with the heat transfer equations, the coupling partial differential Eqs. (1)–(3) are simultaneously solved by the FEM. The calculation starts at time $t = 0$. The initial conditions for both electrons and phonons are assumed to be room temperature. Thus

$$T_e(x, 0) = T_p(x, 0) = 300\,\mathrm{K} \tag{15}$$

In the present model for the two temperature relaxation, the thermionic emission is taken as surface electron heat loss boundary condition on the front surface of the gold film described as

$$K_e \left.\frac{\partial T_e}{\partial x}\right|_{x=0} = -(E_f + e\phi)J\big|_{x=0} \tag{16}$$

where $E_f + e\phi$ is the potential barrier for an electron to be removed from gold material surface. The electrons and phonons heat radiation to the front surface can be neglected during the two temperature relaxation in the femtosecond-to-picosecond time period. And we assume the perfect thermal insulation between the gold film with substrate, leading to

$$\left.\frac{\partial T_e}{\partial x}\right|_{x=d} = \left.\frac{\partial T_p}{\partial x}\right|_{x=d} = 0 \tag{17}$$

For the thermal diffusion relaxation period on ns timescale, which is comparable to heat radiation cycle, so we treat the radiation heat loss to the front surface as a built-in heat loss term as referred in Eq. (3). For the rear surface of gold film, although a small quantity of heat energy can actually arrive at the rear surface, it is almost impossible for the weak heat wave to substantially pass through the rear interface getting into the substrate during the thermal diffusion period because of the large thermal resistance between rear surface of the gold film and the substrate. Therefore, it is appropriate to apply the thermal insulation conditions for electrons and phonons at the rear surface of the gold film in the thermal diffusion relaxation period.

Table 1
Modeling parameters for gold.

Parameters	Value
Material constant χ	353 (W/mK)[a]
Material constant η	0.16[a]
Coefficient for electron heat capacity B_e	70 (J/m^{3}K)[b]
Material constant A_e	1.2×10^7(K^{-2} s^{-1})[c]
Material constant B_p	1.23×10^{11}(K^{-1} s^{-1})[c]
Electron–phonon coupling strength at room temperature G_0	2.20×10^{16}(W/m^3 K)[c]
Ballistic transfer length δ_b	105 nm[d]
Melting point T_m	1336 (K)
Work function ϕ	4.2 eV[e]
Fermi temperature T_F	6.42×10^4(K)

[a] Ref. [24].
[b] Ref. [25].
[c] Ref. [22].
[d] Ref. [29].
[e] Ref. [26].

3. Results and discussion

The physical parameters used for calculations of the thermionic emission properties on gold film are listed in Table 1. The temporal evolution of thermionic emission rates for three laser parameters of laser fluence, laser wavelength and pulse duration with different values are presented in Fig. 1. We can clearly see from Fig. 1(a) that the thermionic emission rates evolution present distinct tendencies for different fluences. For laser fluence of 0.45 J/cm^2, the thermionic emission rate profile is definitely divided into two parts across the timescale of 1 ns. However, for laser fluence of 0.15 J/cm^2, the thermionic emission rate profile emerges as a square wave like shape with pulse duration of 7.9 ps. The physics mechanisms included in regulating the thermionic emission profiles for different laser fluences can actually be related to the thermal relaxation processes in gold film. When laser fluence is high enough for excitation of the thermal diffusion relaxation participating in thermionic emission, the rate profile takes on the two-part structure. On the contrary, as the two temperature relaxation plays a whole role, then the thermionic emission rate profile presents a square wave like shape. It can be seen from Fig. 1(b), that the thermionic emission rate profiles appear as the separate modes as similar in Fig. 1(a) for different laser wavelengths. The corresponding two-part structure for 300 nm wavelength can be attributed to the absorption enhancement of laser irradiation by free electron. It is clearly shown from Fig. 1(c) that thermionic emission profile takes on two-part structure for pulse duration of 100 fs, however, which appears as a Gaussian type impulse by laser excitation with pulse duration of 5 ps. In fact, the femtosecond pulse can effectively heats metal target compared to the picosecond pulse as had been observed in the previous experiment [27], which potentially causes high temperature on gold film surface after two temperature relaxation termination, leading to the thermal diffusion participating in the thermionic emission processes after the two temperature relaxation and the two parts structure formation.

In fact, there should exist the critical laser irradiation conditions for dividing the distinct thermionic emission regimes exhibiting as different thermionic emission rate profiles. Fig. 2 presents predictions of laser wavelength dependence of critical pulse duration for dividing the distinct regimes of thermionic emission on gold film surface. It is obviously shown that total region of the chart can be separated into two parts by the curve marked by separate laser fluences. The region below the curve represents laser parameters for

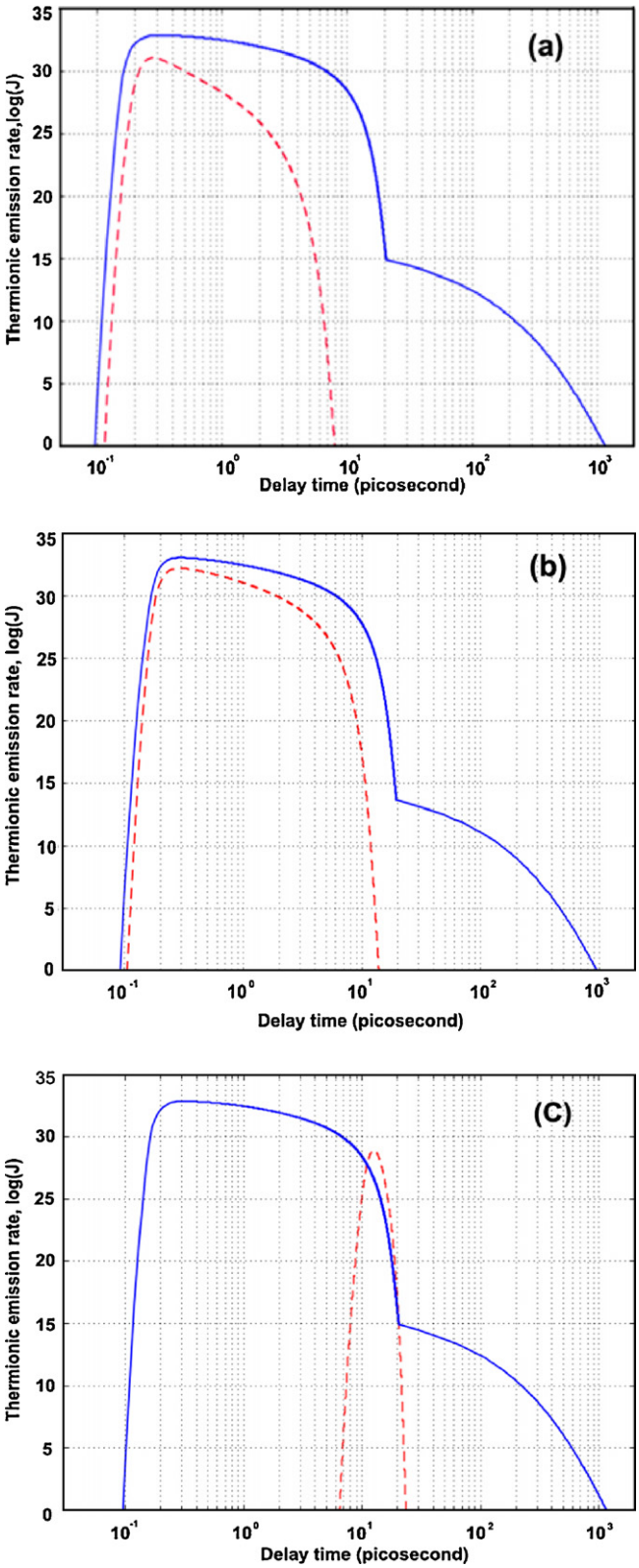

Fig. 1. Temporal evolution of thermionic emission rates for three laser parameters of laser fluence, laser wavelength and pulse duration with different values. (a) The solid line represents for laser fluence $F = 0.45\,J/cm^2$, the dashed line represents for laser fluence $F = 0.15\,J/cm^2$, laser wavelength $\lambda = 800\,nm$, pulse duration $t_p = 100\,fs$; (b) the solid line represents for laser wavelength $\lambda = 300\,nm$, the dashed line represents for laser wavelength $\lambda = 800\,nm$, laser fluence $F = 0.25\,J/cm^2$, pulse duration $t_p = 100\,fs$; (c) the solid line represents for pulse duration $t_p = 100\,fs$, the dashed line represents for pulse duration $t_p = 5\,ps$, laser wavelength $\lambda = 800\,nm$, laser fluence $F = 0.45\,J/cm^2$.

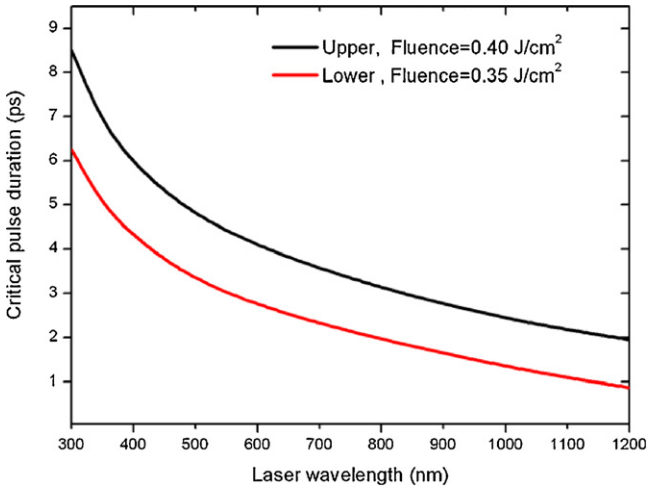

Fig. 2. Laser wavelength dependence of the critical pulse duration for dividing the regimes of thermionic emission on gold film surface.

excitation of thermionic emission rate profiles exhibiting as two-part structure across the timescale of several ns. The region above the curve relates to the regime of thermionic emission dominated by two temperature relaxation, in which the ultrafast electron pulse with picosecond duration such as the square wave or Gaussian type outlines can be generated. More interesting to our concerns, it is found that the curves marked by the laser fluence can be shifted almost parallel to each other by changing the laser fluence as shown for $0.35\,J/cm^2$ and $0.4\,J/cm^2$. When one expects to restrict the thermionic emission properties into the desired regime, it is convenient to locate the all laser pulse parameters in the chart. It indicates that the thermionic emission properties can be influenced and transited from one regime to another under different laser irradiation conditions of laser fluence, wavelength and pulse duration. It should be emphasized that the thermionic emission yield is smaller during the thermal diffusion relaxation compared to two temperature relaxation period, however, the thermionic emission rate would be quite high after the two temperature relaxation termination. So it calls for the necessary to investigate the thermionic emission regimes under the two temperature relaxation and thermal diffusion relaxation for optimizing the ultrashort thermionic pulse shapes. In the following, we will pay more attention on examining the effect of laser parameters on thermionic emission yields in the regime for generation of single peak picosecond pulse electrons shape.

The predictions of thermionic emission yields and maximal phonon temperature as functions of laser fluence are shown in Fig. 3. It is obviously seen that the phonon temperature presents an obvious raise with increasing laser fluence and the thermionic emission yield increases significantly when laser fluence increases in regime of low fluence. However, as laser fluence exceeds $0.17\,J/cm^2$, the thermionic emission yield trends to get saturation. The results can be explained as significant intervention of laser fluence into gold film thermal relaxation dynamics. The high laser fluence can lead to the dramatic increase of the two temperature relaxation time, indicating the thermionic yield increases significantly when fluence increases as a result of the long thermionic emission period. However, as the laser fluence is high enough that the laser thermal energy diffusion into gold film predominates over thermionic emission, the thermionic electron yield trends to get saturation when laser fluence exceeds $0.17\,J/cm^2$.

Fig. 4 shows the thermionic emission yields and maximal phonon temperature as functions of pulse durations. We can see that the thermionic emission yield decreases slowly with increasing pulse duration in the femtosecond time regime. How-

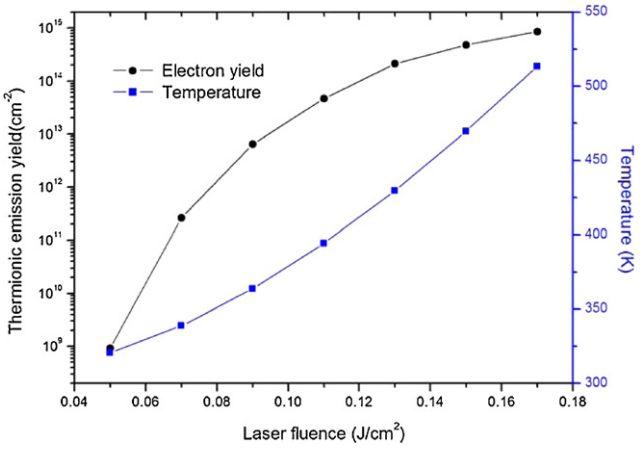

Fig. 3. The thermionic emission yields and the maximal phonon temperature on gold film surface as functions of laser fluence. Pulse duration t_p = 30 fs, laser wavelength λ = 800 nm.

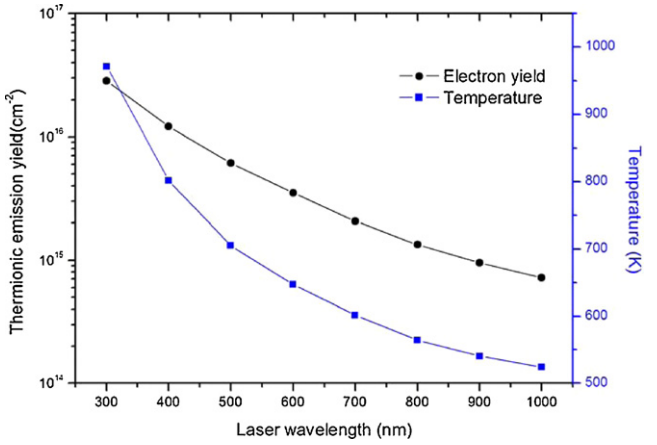

Fig. 5. The thermionic emission yield and the maximal phonon temperature on gold film surface as functions of laser wavelength. Laser fluence F = 0.20 J/cm^2, pulse duration t_p = 100 fs.

ever, in picosecond time domain, the increase of pulse duration will results in sharp drop of the thermionic emission yield. It indicates that the thermionic emission yield under femtosecond laser pulse excitation is more stable compared to picosecond pulse even though the laser pulse duration is subjected to perturbation due to material dispersion, which is potentially beneficial for application of the high quality photocathodes. The phonon temperature is found to bear similar regulation as the thermionic emission yield dependence on pulse duration.

Fig. 5 presents the thermionic emission yield and the maximal phonon temperature on gold film surface as functions of laser wavelengths. It is shown that the thermionic emission yield and maximal phonon temperature decreases violently with increasing laser wavelength. The obvious decrease of thermionic emission yield with increasing laser wavelength can also be attributed to the reduction of surface electron temperature due to laser absorption weakening on the gold film surface under the long wave excitation.

In the above investigations, we had ruled out the effect of the SC effect in order to obtain the high electron yield and get the insights into the intrinsical characteristics of thermionic emission regime under a femtosecond laser pulse. However, as the surface electron temperature of metal is high enough that a large region of the electron cloud is formed over the surface, the space–charge effect would play an important role. Experimentally, one can overcome SC suppression of the yield by biasing the emitter at a negative potential with respect to a nearby anode. Herein, we estimated the effect of SC on the thermionic emission characteristics. The results show that for the 30 fs laser pulse excitation with fluence of 0.2 J/cm^2, the SC limited yield on gold film is approximately 5-order of magnitude smaller than that without the SC effect. In order to negate the SC effect, the external biasing potential must be on the order of 10^7–10^8 V [23].

Fig. 6 shows dependence of the calculated melting thresholds on gold film thickness and the comparisons to experimental results. We applied the two temperature model (TTM) in cooperation with space charge limited thermionic emission model to predict the gold film melting thresholds for different thickness. For the femtosecond laser damage threshold investigations. It is reasonable to assume that the hydrodynamics process can be ignored because of the quite longer hydrodynamics period compared to the electron–phonon heating period (several picosecond seconds for gold). Here, we had ignored the pressure relaxation process and only ultrafast heat transfer is taken into account to explain the gold melting threshold as a result of isochoric heating upon a femtosecond pulse. In this

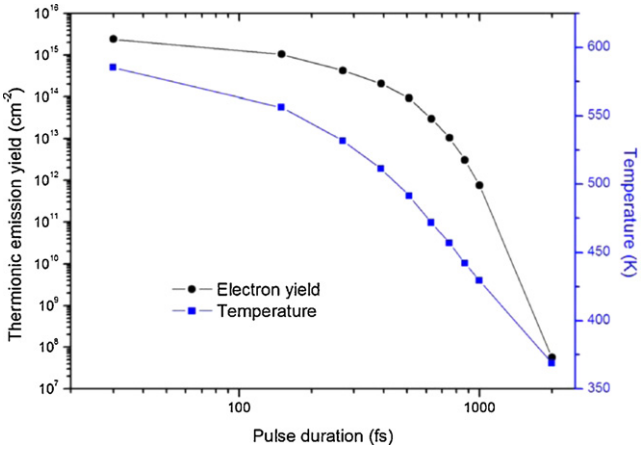

Fig. 4. The thermionic emission yield and maximal phonon temperature on gold film surface as functions of pulse durations. Laser fluence F = 0.20 J/cm^2, laser wavelength λ = 800 nm.

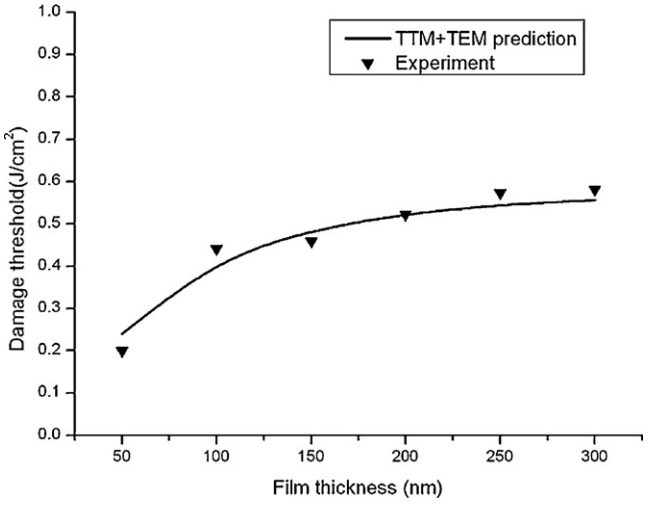

Fig. 6. The dependence of the calculated melting thresholds on gold film thickness and the comparisons to experimental results, laser wavelength λ = 1053 nm, pulse duration t_p = 600 fs.

regime, the target can be overheated to some degree evaluated by the overheating parameter of $\alpha = T/T_m$. In current simulations, the α is taken as 1.3 for gold target. The thermionic emission under the two temperature relaxation during the ablation is taken into account as the thermal loss boundary conditions from the front surface of the gold film. However, the thermionic emission during the thermal diffusion is normally ignored because the target had been ablated after two temperature relaxation termination in high laser fluence regime, the broken surface of the target is not qualified for the sequential thermionic emission. The simulated results of gold film melting thresholds present excellent accordance with published experimental datum [28], which proves validity of predictions of the thermionic emission properties on gold film surface.

4. Conclusions

The results showed that the thermionic electron pulse profiles could exhibit various shapes, intricately depending on laser irradiation parameters. A chart for dividing the distinct thermionic emission regimes dominated by the different thermal relaxation was obtained, in which the single peak and the two-part structure thermionic emission rate profiles can be well defined by limiting the laser irradiation parameters of laser fluence, pulse duration and laser wavelength. It was demonstrated that the thermionic emission rate profile properties could be transited from one regime to another under different laser parameters. The characteristics of thermionic electron yield under two temperature relaxation for picosecond thermionic electron profiles were carefully examined, which showed that the thermionic emission yields increases obviously with increasing laser fluence and gets saturated in high laser fluence regime. The results provide way for optimizing thermionic emission processes for generation of ultrashort thermionic electron pulse.

Acknowledgements

The work was supported by National High Technology R&D Program of China under the grant no. 2009AA04Z305 and National Science Foundation of China under the grant no. 60678011.

References

[1] J. Dunn, A.L. Osterheld, R. Shepherd, W.E. White, V.N. Shlyaptsev, R.E. Stewart, Phys. Rev. Lett. 80 (1998) 2825.
[2] S.W. Downey, L.A. Builta, D.C. Moir, T.J. Ringler, J.D. Saunders, Appl. Phys. Lett. 49 (1986) 911.
[3] E. Räsänen, A. Castro, J. Werschnik, A. Rubio, E.K.U. Gross, Phys. E 40 (2008) 1593.
[4] L.M. Chen, J.J. Park, K.-H. Hong, J.L. Kim, J. Zhang, C.H. Nam, Phys. Rev. E 66 (2002) 025402 (R).
[5] A. Gloskovskii, D.A. Valdaitsev, M. Cinchetti, S.A. Nepijko, J. Lange, M. Aeschlimann, M. Bauer, M. Klimenkov, L.V. Viduta, P.M. Tomchuk, G. Schönhense, Phys. Rev. B 77 (2008) 195427.
[6] P. Muggli, R. Brogle, C. Joshi, J. Opt. Soc. Am. B 12 (1995) 553.
[7] J.P. Girardeau-Montaut, C. Girardeau-Montaut, S.D. Moustaizis, C. Fotakis, Appl. Phys. Lett. 62 (1993) 426.
[8] J. Cao, Y. Gao, H.E. Elsayed-Ali, R.J.D. Miller, D.A. Mantell, Phys. Rev. B 58 (1998) 10948.
[9] L.M. Chen, J. Zhang, Q.L. Dong, H. Teng, T.J. Liang, L.Z. Zhao, Z.Y. Wei, Phys. Plasmas 8 (2001) 2925.
[10] U. Teubner, I. Uschmann, P. Gibbon, D. Altenbernd, E. Fröster, T. Feurer, W. Theobald, R. Sauerbrey, G. Hirst, M.H. Key, J. Lister, D. Neely, Phys. Rev. E 54 (1996) 4167.
[11] T.H. Ning, C.M. Osburn, H.N. Yu, J. Appl. Phys. 84 (1977) 286.
[12] S.S. Mao, X. Mao, J.H. Yoo, R. Greif, R.E. Russo, J. Appl. Phys. 83 (1998) 4462.
[13] T. Balasubramni, S.H. Kim, S.H. Jeong, Appl. Surf. Sci. 255 (2009) 9601.
[14] Guangqing Du, Feng Chen, Qing Yang, Jinhai Si, Xun Hou, Opt. Commun. 283 (2010) 1869.
[15] N.M. Bulgakova, I.M. Bourakov, Appl. Surf. Sci. 197–198 (2002) 41.
[16] M. Bonn, N. Daniel, Denzler, S. Funk, M. Wolf, S.-S. Wellershoff, J. Hohlfeld, Phys. Rev. B 61 (2000) 1101.
[17] L. Jiang, H.L. Tsai, Int. J. Heat Mass Transfer 50 (2007) 3461.
[18] A.P. Kanavin, I.V. Smetanin, V.A. Isakov, Yu.V. Afanasiev, B.N. Chichkov, B. Wellegehausen, S. Nolte, C. Momma, A. Tünnermann, Phys. Rev. B 57 (1998) 14698.
[19] J.P. Colombier, P. Combis, F. Bonneau, R. Le Harzic, E. Audouard, Phys. Rev. B 71 (2005) 165406.
[20] Lan Jiang, Hai-Lung Tsai, J. Appl. Phys. 104 (2008) 093101.
[21] J.K. Chen, D.Y. Tzou, J.E. Beraun, Int. J. Heat Mass Transfer 49 (2006) 307.
[22] Y. Zhang, J.K. Chen, Appl. Phys. A 88 (2007) 289.
[23] D.M. Riffe, X.Y. Wang, M.C. Downer, D.L. Fisher, T. Tajima, J.L. Erskine, R.M. More, J. Opt. Soc. Am. B 10 (1993) 1424.
[24] J.K. Chen, W.P. Latham, J.E. Beraun, Numer. Heat Transfer Part B 42 (2002) 1.
[25] T.Q. Qiu, C.L. Tien, J. Heat Transfer 115 (1993) 835.
[26] G.V. Samsonov (Ed.), Physicochemical Properties of the Elements, Naukova Dumka, Kiev, 1965 (in Russian).
[27] A. Ancona, S. Döring, C. Jauregui, F. Röser, J. Limpert, S. Nolte, A. Tünnermann, Opt. Lett. 34 (2009) 3304.
[28] B.C. Stuart, M.D. Feit, S. Herman, A.M. Rubenchik, B.W. Shore, M.D. Perry, J. Opt. Soc. Am. B 13 (1996) 459.
[29] S.-S. Wellershoff, J. Hohlfeld, J. Güdde, E. Matthias, Appl. Phys. A 69 (Suppl.) (1999) S99.